

as well as nanotubes partially or completely filled with Ga, thus forming coaxial nanocables. By optimizing the reaction conditions, e.g., carefully selecting deposition temperature, it is believed that the present method can be used to grow crystalline Ga₂O₃-ZnO coaxial nanotubes and Ga-filled coaxial nanocables, which are expected to have interesting electronic and photonic properties.

Experimental

The Ga-filled Ga₂O₃-ZnO composite coaxial nanotubes were synthesized in a vertical induction furnace with a susceptor made of graphite, as described in detail elsewhere [12]. Briefly, the induction furnace consists of a clear fused-quartz tube (50 cm in length, 12 cm in outer diameter, and 0.25 cm in wall thickness) and an inductively heated cylinder of high purity graphite (25 cm in length, 4.5 cm in outer diameter, and 3.5 cm in inner diameter). The inductively heated cylinder, which was coated with a C fiber thermal insulating layer, had one inlet C pipe and outlet C pipe on its top and base, respectively. The inductively heated cylinder together with the thermal insulating layer was screened inside the fused-quartz tube. A mixture of Ga₂O₃ powder (0.5 g, 99.9%, Aldrich) and ZnO powder (1.2 g, 99.9%, Aldrich) was placed on an uncover graphite C crucible (2.5 cm in outer diameter, 3 mm in wall thickness, and 2 cm in height). After transferring the C crucible containing the starting material to the center of the inductively heated cylinder, the quartz tube was evacuated by a mechanical rotary pump to a pressure of about 5×10^{-1} torr. During the experiment, a pure Ar flow was introduced through the tube at a flow rate of 80 sccm and the ambient pressure in the tube. The mixture in the crucible was heated to and maintained at 1350 °C (measured by an optical pyrometer with an estimated accuracy of ± 10 °C) for 2 h. After the reaction was terminated and the furnace cooled to room temperature, the collected product was characterized using transmission electron microscopy (TEM; JEM-3000F) with an X-ray energy dispersive spectrometer (EDS). The photoluminescence spectra were measured at room temperature in the spectral range of 350–800 nm using a He–Cd laser with a wavelength of 325 nm as the excitation source.

Received: January 6, 2003
Final version: March 15, 2003

- [1] a) L. E. Brus, *J. Phys. Chem.* **1994**, *98*, 3575. b) C. B. Murray, C. R. Kagan, M. G. Bawendi, *Science* **1995**, *270*, 1335. c) D. Snoke, *Science* **1996**, *273*, 1351. d) B. I. Yacobson, R. E. Smalley, *Am. Sci.* **1997**, *85*, 324. e) J. Hu, M. Yang, P. Yang, C. M. Lieber, *Nature* **1999**, *399*, 48. f) C. Dekker, *Phys. Today* **1999**, *52*, 22. g) J. Hu, T. W. Odom, C. M. Lieber, *Acc. Chem. Res.* **1999**, *32*, 435.
- [2] P. Szuromi, *Science* **1998**, *281*, 881.
- [3] a) Y. Zhang, K. Suenaga, C. Colliex, S. Iijima, *Science* **1998**, *281*, 973. b) Y. Zhang, H. Gu, K. Suenaga, S. Iijima, *Chem. Phys. Lett.* **1997**, *279*, 264.
- [4] W. Shi, H. Peng, L. Xu, N. Wang, Y. Tang, S. T. Lee, *Adv. Mater.* **2000**, *12*, 1927.
- [5] K. Suenaga, C. Colliex, N. Demoncey, A. Loiseau, H. Pascard, F. Willaime, *Science* **1997**, *278*, 653.
- [6] a) P. M. Ajayan, S. Iijima, *Nature* **1993**, *361*, 333. b) C. Guerret-Piécourt, Y. Le Bouar, A. Loiseau, H. Pascard, *Nature* **1994**, *372*, 761. c) S. C. Tsang, Y. K. Chen, P. J. F. Harris, M. L. H. Green, *Nature* **1994**, *372*, 159. d) P. M. Ajayan, O. Stephan, P. Redlich, C. Colliex, *Nature* **1995**, *375*, 564. e) D. Ugarte, A. Chatelain, W. A. De Heer, *Science* **1996**, *274*, 1897. f) M. Terrones, W. K. Hsu, A. Schilder, H. Terrones, N. Grobert, J. P. Hare, Y. Q. Zhu, M. Schwoerer, K. Prassides, H. W. Kroto, D. R. M. Walton, *Appl. Phys. A: Mater. Sci. Process.* **1998**, *66*, 307. g) J. Sloan, J. Cook, M. L. H. Green, J. L. Hutchison, R. Tenne, *J. Mater. Chem.* **1997**, *7*, 1089.
- [7] a) J. Hu, Q. Li, N. B. Wong, C. S. Lee, S. T. Lee, *Chem. Mater.* **2002**, *14*, 1216. b) J. Hu, Q. Li, X. Meng, C. S. Lee, S. T. Lee, *J. Phys. Chem. B* **2002**, *106*, 9536. c) D. S. Ginley, C. Bright, *Mater. Res. Soc. Bull.* **2000**, *25*, 15. d) A. M. Morales, C. M. Lieber, *Science* **1998**, *279*, 208.
- [8] C. H. Liang, G. W. Meng, G. Z. Wang, Y. W. Wang, L. D. Zhang, S. Y. Zhang, *Appl. Phys. Lett.* **2001**, *78*, 3202.
- [9] a) W. Q. Han, S. S. Fan, Q. Q. Li, Y. D. Hu, *Science* **1997**, *277*, 1287. b) H. Y. Peng, X. T. Zhou, N. Wang, Y. F. Zheng, L. S. Liao, W. S. Shi, C. S. Lee, S. T. Lee, *Chem. Phys. Lett.* **2000**, *327*, 263.
- [10] J. Q. Hu, Q. Li, X. M. Meng, C. S. Lee, S. T. Lee, *J. Phys. Chem. B* **2002**, *106*, 9536.
- [11] Y. H. Gao, Y. Bando, D. Golberg, *Appl. Phys. Lett.* **2002**, *81*, 4133.

- [12] a) D. Golberg, Y. Bando, L. Bourgeois, K. Kurashima, T. Sato, *Carbon* **2000**, *38*, 2017. b) D. Golberg, Y. Bando, W. Q. Han, K. Kurashima, T. Sato, *Chem. Phys. Lett.* **1999**, *308*, 337. c) W. Q. Han, Y. Bando, K. Kurashima, T. Sato, *Appl. Phys. Lett.* **1998**, *73*, 3085.

High-Density 40 nm Diameter Sb-Rich Bi_{1-x}Sb_xTe₃ Nanowire Arrays**

By Marisol Martín-González,* Amy L. Prieto, Ronald Gronsky, Timothy Sands, and Angelica M. Stacy

There is renewed interest in thermoelectric materials because of the promise that quantum confinement will increase the efficiencies of these materials compared with bulk.^[1] A three- to four-fold increase in the figure of merit for these materials is necessary in order to compete with compressor-based refrigerators, although more modest increases would still have a substantial impact on many applications.^[2] Bi_{0.5}Sb_{1.5}Te₃ is among the preferred thermoelectric materials for applications near room temperature, which makes this material one of the best targets for the synthesis of nanowires.^[3]

A single nanowire is not able to transport enough current to make a workable device. We therefore fill templates using electrodeposition in order to fabricate large-scale ordered arrays of nanowires,^[4] exploiting the templates not only for the size and order of the pores, but also for their beneficial mechanical stability. Prior work has shown that the electrodeposition of (Bi_{1-x}Sb_x)₂Te₃ films is quite challenging. It is difficult to achieve a sufficiently high concentration of Sb in an aqueous solution,^[5] and there is not much published information on appropriate chelating agents or their concentrations. Also, the stoichiometric films obtained by electrodeposition^[5] are highly porous and exhibit dendritic growth when deposition is performed at potentials more negative than -0.12 V versus the standard calomel electrode (SCE)^[5] and for low concentrations of Sb. Here, we report the synthesis of dense 40 nm nanowire arrays of (Bi_{1-x}Sb_x)₂Te₃. At diameters of 40 nm, it is reasonable to anti-

[*] Dr. M. Martín-González,^[+] Dr. A. L. Prieto,^[++] Prof. A. M. Stacy
Department of Chemistry, University of California
Berkeley, CA 94720 (USA)
E-mail: marisol@imm.cnm.csic.es
Prof. R. Gronsky, Prof. T. Sands^[+++]
Department of Materials Science and Engineering
University of California
Berkeley, CA 94720 (USA)

[+] Current address: Instituto de Microelectrónica de Madrid, IMM (CNM-CSIC) C/Isaac Newton, 8 (PTM), E-28760-Tres Cantos, Madrid, Spain.

[++] Current address: Department of Chemistry and Chemical Biology, Harvard University, 12 Oxford Street, Cambridge, MA 02138, USA.

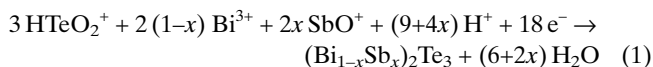
[+++] Current address: School of Materials Engineering, School of Electrical and Computer Engineering, and the Birk Nanotechnology Center, Purdue University, 501 Northwestern Ave., West Lafayette, IN 47907-2036, USA.

[**] This work was funded by the Department of Defense ONR-MURI on thermoelectrics, contract number N00014-97-1-0516. M.S.M.G thanks the MEC/Fulbright postdoctoral fellowship program and A.L.P. thanks Bell Labs, Lucent Technologies for funding. The authors would also like to thank Prof. Jeffrey Long and his group for the use of the bioanalytical systems Basomatic CV50W and Ron Wilson (Department of Materials Science, UCB) and for help with the SEM. We also thank the electron microscope laboratory and microfabrication laboratory for use of their facilities.

pate phonon-dampening effects, which should lead to an enhanced thermoelectric response. The individual wires are crystalline and highly oriented after thermal treatment, with diameters of 40 nm and a composition of $\text{Bi}_{0.6}\text{Sb}_{1.6}\text{Te}_{2.8}$ (close to $\text{Bi}_{0.5}\text{Sb}_{1.5}\text{Te}_3$, the best composition for thermoelectric performance). In the process of producing these 40 nm nanowires, the relevant electrodeposition mechanisms were established for films as well as thicker (200 nm) wire arrays.

We have expanded upon previous work^[5] to develop a working electrolyte. The procedure begins with dissolving elemental Te and Bi in concentrated nitric acid. Next, SbCl_3 is dissolved in a separate beaker using tartaric acid to increase the Sb solubility in water by forming Sb–tartaric complexes. Once the solids are dissolved in both beakers they are mixed together and water is added to reach the final volume. The final composition of the solution is HTeO_2^+ (1×10^{-2} M), Bi^{3+} (0.19×10^{-2} M), SbO^+ (0.56×10^{-2} M), and tartaric acid (0.84 M) in HNO_3 (1 M). The Sb precursor must be dissolved in the presence of the tartaric acid before addition to the Bi and Te solution in order to achieve the correct solubility.

Cyclic voltammograms for solutions with and without Sb plus tartaric acid are compared in Figure 1. The overall $(\text{Bi}_{1-x}\text{Sb}_x)_2\text{Te}_3$ electrodeposition reaction can be described as:



For simplicity, the complexing agent (tartaric acid) has been omitted from Equation 1.

The reduction processes for the solution containing Sb plus tartaric (solid line) are comparable in shape to those observed without (dashed line). There are two reduction processes in both cases, associated with two different mechanisms which follow the general reaction given by Equation 1. In the case of solutions containing Sb, the deposition takes place by the electrochemically induced reduction of HTeO_2^+ to Te^0 for the

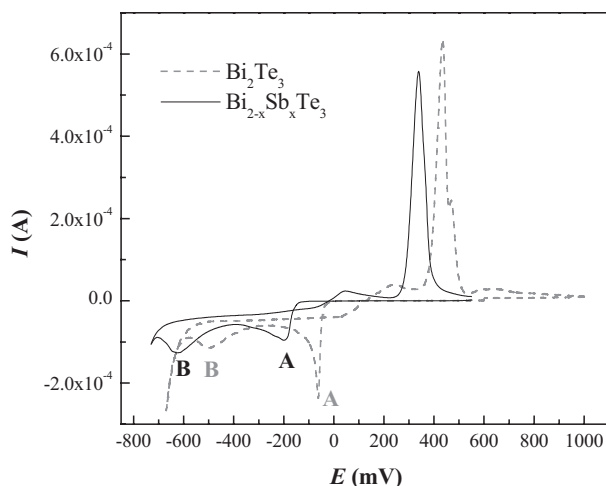


Fig. 1. Cyclic voltammograms of (solid line) Bi^{3+} (0.75×10^{-2} M) and HTeO_2^+ (1×10^{-2} M) in HNO_3 (1 M) and (dashed line) HTeO_2^+ (1×10^{-2} M), Bi^{3+} (0.19×10^{-2} M), SbO^+ (0.56×10^{-2} M), tartaric acid (0.84 M) and HNO_3 (1 M) solution. Scan rate = 0.01 V s^{-1} , reference electrode Ag/AgCl (3 M NaCl), room temperature in both cases.

first reduction peak (~ -0.20 V vs. Ag/AgCl) and to H_2Te for the second (~ -0.625 V vs. Ag/AgCl). After this electrochemical reduction there is a reaction with Bi^{3+} and SbO^+ in solution to give the final compound since the compound is more stable than Te^0 or H_2Te .^[6] The shift of the reduction potentials to more negative values upon the addition of the Sb–tartaric complex is consistent with the fact that complexed cations are generally reduced at more negative reduction potentials than isolated cations. A more detailed study of the electrodeposition mechanism for Bi_2Te_3 ^[6–8] was published elsewhere.^[6] We conclude that for our solution, the deposition of $(\text{Bi}_{1-x}\text{Sb}_x)_2\text{Te}_3$ is favorable at potentials more negative than ~ -0.17 V versus Ag/AgCl on Pt as a working electrode, but a second mechanism for deposition appears once the potential is more negative than ~ -0.5 V.

Films were prepared in order to examine the best composition, homogeneity, and crystallinity of the deposited material as a function of reduction potential, so the optimal deposition conditions for films could be used as a starting point for the deposition of nanowires in the alumina templates. When the potential was held at ~ -0.2 V versus Ag/AgCl, a dark deposit was observed on the Ag electrode. Energy dispersive spectroscopy (EDS) analysis of these films confirmed the substitution of about 79 % of the Bi with Sb. The error associated with EDS is within 3–5 at.-%. The powder X-ray diffraction (XRD) pattern for the deposits indicated one set of lines that could be indexed to the rhombohedral space group, $R\bar{3}m$ (166), for the $\text{Bi}_{0.5}\text{Sb}_{1.5}\text{Te}_3$ structure type (JCPDS 49-1713), indicating that a single phase had been formed. Taken together, the EDS and XRD results indicate that the electrodeposited films are single phase with an approximate composition of $\text{Bi}_{0.8}\text{Sb}_{1.2}\text{Te}_3$ or $(\text{Bi}_{0.4}\text{Sb}_{0.6})_2\text{Te}_3$, close to the $\text{Bi}_{0.5}\text{Sb}_{1.5}\text{Te}_3$ composition currently used in thermoelectric devices.^[2]

Nanowire arrays of 200 nm diameter were prepared using commercially available porous alumina. Ag was sputtered onto one side of the alumina, and the alumina/Ag composite was used as the working electrode. The templates became uniformly dark in color during deposition. The deposition was allowed to continue until an increase in the current was observed, indicating that the deposition was occurring on the top surface. The composition of the deposit as determined by EDS was roughly $\text{Bi}_{0.7}\text{Sb}_{1.4}\text{Te}_{2.9}$ or $(\text{Bi}_{0.35}\text{Sb}_{0.7})_2\text{Te}_{2.9}$, similar to that observed for films and closer to the ideal “x” value. After mechanically polishing the Ag electrode off the bottom surface, scanning electron microscopy (SEM) images revealed that ~ 75 % of the pores were filled with $\text{Bi}_{0.7}\text{Sb}_{1.4}\text{Te}_{2.9}$.

A very interesting phenomenon is observed when growing this phase into porous alumina. The wires do not wet the alumina, as is evident by the gap between the wires and the pore walls. This non-wetting behavior is not detected for the deposition of pure Bi_2Te_3 ,^[8,9] but is detected for $\text{Bi}_{1-x}\text{Sb}_x$ alloys.^[10] Consequently, we believe the non-wetting is due to the presence of Sb. Nevertheless, as can be seen in Figure 2, slowing down the electrodeposition rate can reduce the gap. A cross-sectional image reveals very little gap between the alumina walls and the wires. The individual wires are continu-

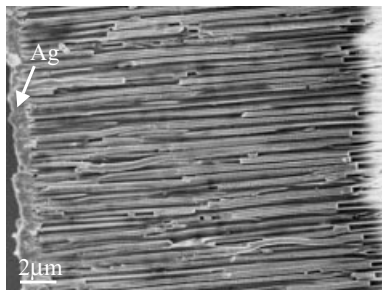


Fig. 2. SEM image of a cross-section of a 200 nm $\text{Bi}_{0.7}\text{Sb}_{1.4}\text{Te}_{2.9}$ wire array showing 16 μm long wires with no gap between the alumina and the wires.

ous and dense. As can also be seen in Figure 2, all the wires are the same length, indicating that they nucleated at the same time. The XRD patterns for the 200 nm wire arrays are similar to those described above for films, indicating that the wires are polycrystalline and single phase, with a composition close to $\text{Bi}_{0.5}\text{Sb}_{1.5}\text{Te}_3$.

Obtaining high quality 40 nm wires arrays is significantly more challenging. First, high-quality alumina templates must be fabricated. These are not commercially available and they are more fragile than the commercial 200 nm ones. We have fabricated the templates using a procedure published previously, which is based on several prior reports.^[11]

The 40 nm templates became dark in color during deposition. The depositions were carried out under fast and slow growth conditions for comparison. Under fast growth with applied potentials more negative than -0.17 V versus Ag/AgCl, the “nanowires” are very rough and highly porous, indicative of cellular or dendritic growth (Fig. 3a). When slow growth conditions are used, $E \sim -0.17$ V versus Ag/AgCl, we find again that the wires do not fill the pore completely, as shown in Figure 3b, however, the wires are smooth and fairly uniform in diameter. This is an interesting phenomenon since we can achieve wires with smaller diameter than the pore size, if needed. Around 80 % of the pores are filled with $\sim 30 \mu\text{m}$ long wires. EDS analysis in the SEM of the cross-section indicates that the composition of the 40 nm nanowire array is roughly 12 % Bi, 32 % Sb, and 56 % Te, ($\text{Bi}_{0.6}\text{Sb}_{1.6}\text{Te}_{2.8}$).

The XRD patterns obtained for 40 nm nanowires arrays are similar to those of films and 200 nm arrays (Fig. 4). The peaks are shifted as expected for the level of alloying observed. If the sample is annealed at 300°C (Fig. 4, top), an increase in the intensity of the 110 peak is observed, indicating an increase in the texturing along that direction. This is the orientation yielding the highest thermoelectric performance for $\text{Bi}_{0.5}\text{Sb}_{1.5}\text{Te}_3$.

We conclude that electrodeposition at potentials more negative than $E = -0.17$ V versus Ag/AgCl of a solution containing Te, Bi, Sb, and tartaric and nitric acids gives rise to the formation of films and wires of $(\text{Bi}_{1-x}\text{Sb}_x)_2\text{Te}_3$ with $x \sim 0.7$. The films are polycrystalline and single-phase. A non-wetting effect between the alumina and the wires containing Sb is observed. Slowing down the electrodeposition rate partially compensates for the poor wetting of the template by the wire material. Slow deposition rates produce high-quality nanowires with high aspect ratios ($\sim 10^3$) and which completely fill the pores. From

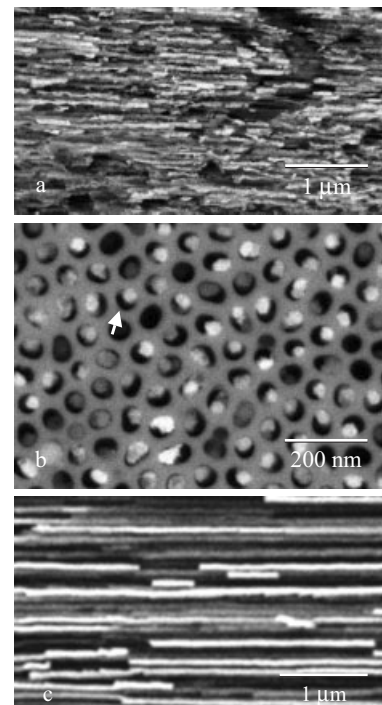


Fig. 3. Backscattering micrograph of a) cross-section of a 40 nm array filled with Bi/Sb/Te indicating rapid growth, b) top view, after polishing the Ag off, of a sample grown at moderate deposition rate and c) cross-section of (b). A gap (indicated by an arrow) is observed between the nanowire of $\text{Bi}_{0.6}\text{Sb}_{1.6}\text{Te}_{2.8}$ (white spots) and the anodized alumina (gray). This behavior is due to a dewetting effect associated with the high Sb concentration in the wire.

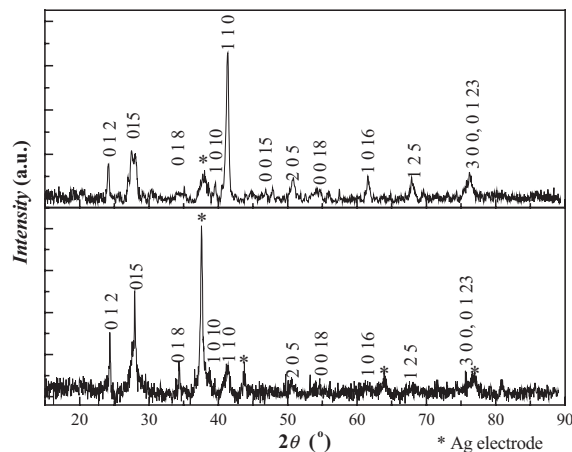


Fig. 4. Comparison between XRD patterns of the same sample after removal of the Ag electrode by mechanically polishing, before heat treatment (bottom) and after heat treatment (top).

the perspective of thermoelectric device performance, a high pore filling fraction is necessary to minimize the detrimental effect of parasitic heat flow through the supporting matrix.

Experimental

Cyclic voltammograms were recorded with a bioanalytical systems Basomatic CV50W unit. A three-electrode electrochemical cell was employed consisting of a Ag/AgCl reference electrode (3 M NaCl, 0.175 V vs. normal hydrogen electrode (NHE)) a Pt disc working electrode and a Pt wire counter electrode. The working electrode was polished and ultrasonically cleaned be-

fore each voltammogram in order to ensure a clean surface for each scan. Solutions of HTeO_2^- (1×10^{-2} M) plus a) Bi^{3+} (0.19×10^{-2} M), SbO^+ (0.56×10^{-2} M), and tartaric acid (0.84 M), and b) Bi^{3+} (0.75×10^{-2} M) both in HNO_3 (1 M), were studied. SbCl_3 (Aldrich, 99.99+%) was dissolved in tartaric acid (0.84 M) (Aldrich, 99 %). Concentrated nitric acid (Fisher, 69.1 %) was used to dissolve the elemental Bi (Mallinckrodt, 99.8 %) and Te (Alfa Aesar, 99.9998 %). The two solutions were combined and water was added to reach the final volume and appropriate concentration for HNO_3 (1 M).

200 nm templates were purchased from Whatman and 40 nm porous alumina templates were prepared in our laboratory [9].

Electrodeposition of $(\text{Bi}_{1-x}\text{Sb}_x)_2\text{Te}_3$ was performed using a standard three-electrode cell (EG&G PAR model 273 potentiostat/galvanostat). The working electrode was prepared by attaching a copper wire to the Pt side of the porous alumina template with Ag paint (Ted Pella, Inc., colloidal silver paste), and the back and edges of the alumina were masked with clear nail enamel. The cathode assembly and anode (Pt gauze) were submerged in the solution. The reference electrode (Ag/AgCl) was in a separate cell in a 1.0 M KNO_3 solution. The two cells were connected via a 1.0 M KNO_3 /agar salt bridge. Depositions of $(\text{Bi}_{1-x}\text{Sb}_x)_2\text{Te}_3$ were performed under potentiostatic control with potentials more negative than ~ -0.17 V versus Ag/AgCl.

The composition and morphology of the films and nanowires arrays were analyzed using several techniques: EDS (JEOL 6300), X-ray diffraction (Siemens D5000, Cu K α radiation), and field-emission SEM (Hitachi S-5000).

Received: December 19, 2002
Final version: March 6, 2003

- [1] a) L. D. Hicks, M. S. Dresselhaus, *Phys. Rev. B* **1993**, *47*, 12727. b) L. D. Hicks, M. S. Dresselhaus, *Phys. Rev. B* **1993**, *47*, 16631. c) L. D. Hicks, T. C. Harman, X. Sun, M. S. Dresselhaus, *Phys. Rev. B* **1996**, *53*, 10493. d) T. C. Harman, D. L. Spears, M. P. Walsh, *J. Electron. Mater.* **1999**, *28*, L1. e) T. C. Harman, P. J. Taylor, D. L. Spears, M. P. Walsh, *J. Electron. Mater.* **2000**, *29*, L1. f) T. C. Harman, P. J. Taylor, M. P. Walsh, B. E. La Forge, *Science* **2002**, *297*, 2229. g) R. Venkatasubramanian, E. Siivola, T. Colpitts, B. O'Quinn, *Nature* **2001**, *413*, 597.
- [2] *CRC Handbook of Thermoelectrics* (Ed: D. M. Rowe), CRC Press, Boca Raton, FL **1995**.
- [3] G. S. Nolas, J. Sharp, H. J. Goldsmith, in *Thermoelectrics: Basic Principles and New Materials Developments*, Springer Verlag, Berlin Heidelberg **2001**, Ch. 5, pp. 123–128.
- [4] C. R. Martin, *Science* **1994**, *266*, 1961.
- [5] J.-P. Fleurial, J. A. Herman, G. J. Snyder, M. A. Ryan, A. Borshchevsky, C. K. Huang, *Mater. Res. Soc. Symp. Proc.* **2000**, *625*, Z11.3.1.
- [6] M. S. Martín-González, A. L. Prieto, R. Gronsky, T. Sands, A. M. Stacy, *J. Electrochem. Soc.* **2002**, *149*, C546.
- [7] P. Magri, C. Boulanger, J. M. Lecuire, *J. Mater. Chem.* **1996**, *6*, 773.
- [8] S. A. Sapp, B. B. Lakshmi, C. R. Martin, *Adv. Mater.* **1999**, *11*, 402.
- [9] A. L. Prieto, M. S. Sander, M. S. Martín-González, R. Gronsky, T. Sands, A. M. Stacy, *J. Am. Chem. Soc.* **2001**, *123*, 7160.
- [10] a) A. L. Prieto, M. S. Martín-González, R. Gronsky, T. Sands, A. M. Stacy, *J. Am. Chem. Soc.* **2003**, *125*, 2388. b) M. S. Martín-González, A. L. Prieto, M. M. Knox, R. Gronsky, T. Sands, A. M. Stacy, *Chem. Mater.* **2003**, *15*, 1676.
- [11] a) C. Miller, *Ph.D. Thesis*, University of California, Berkeley **1987**, p. 271. b) F. Keller, M. S. Hunter, D. L. Robinson, *J. Electrochem. Soc.* **1953**, *100*, 411. c) Z. Zhang, D. Gekhtman, M. S. Dresselhaus, J. Y. Ying, *Chem. Mater.* **1999**, *11*, 1659.

Formidable Increase in the Superplasticity of Ceramics in the Presence of an Electric Field**

By Zhijian Shen,* Hong Peng, and Mats Nygren

Ceramics are brittle materials that break without noticeable plastic deformation at ambient temperatures. When their

[*] Dr. Z. Shen, H. Peng, Prof. M. Nygren
Department of Inorganic Chemistry, BRIIE Center for Inorganic Interfacial Engineering, Arrhenius Laboratory, Stockholm University S-106 91 Stockholm (Sweden)
E-mail: shen@inorg.su.se

[**] This work was supported by the Swedish Research Council through grant 621-2002-4299. We thank Z. Zhao and M. Heinonen for their experimental assistance.

grain size is reduced to a submicrometer level, however, ceramics may become ductile at elevated temperatures.^[1–4] The deformation of ceramics occurs mainly via sliding along grain boundaries; thus the presence of an intergranular glassy phase in conjunction with ultrafine-grained microstructures improves the ductility.^[5–7] For ceramics based on covalently bound Si_3N_4 , the deformation progresses very slowly when the coexisting glassy phase has a high softening temperature and occurs in low concentration,^[3,8,9] and when the constituent grains possess a fibrous morphology.^[10] To enhance the ductility of Si_3N_4 -based ceramics, in particular at lower temperatures, compacts that contain equi-axed submicrometer-sized grains have been prepared by: i) a low-temperature sintering procedure;^[11] ii) adding grain growth inhibitors, such as SiC particles;^[3] and iii) using β - Si_3N_4 powder, because this precursor seems more resistant to grain growth.^[9] The ductility of these types of ceramics is strongly temperature dependent, i.e., it increases with increasing temperature below a certain critical temperature (T_c). Above T_c , the ductility is hindered because the accelerated grain growth induces strain hardening. Strain rates of the order of 10^{-4} s⁻¹ are thus obtained under a compressive stress of 40–50 MPa at temperatures around 1500 °C. Attempts have been made to reduce the viscosity of the grain-boundary glassy phase even further, via compositional adjustment of the glassy phase, in order to lower its softening temperature.^[8] However, the resistance to creep and corrosion is thereby decreased, and these properties which are vital for materials intended for high-temperature applications are sacrificed.

When consolidating Si_3N_4 -based ceramics by spark plasma sintering (SPS), we have observed very fast densification and have obtained fully dense samples within very short times at surprisingly low temperatures, e.g., in the range of 1450–1550 °C.^[12–14] In the SPS process, the powder is loaded in a graphite die and subjected to a uniaxial pressure. The die is heated by passing a pulsed direct current through it. The use of a pulsed current implies that the sample is exposed to a pulsed electric field. One interpretation of the excellent densification results described above is that the viscosity of the liquid/glassy phase was reduced by the electric field. If this is true, one would expect a similar improvement in the deformation rate. We have accordingly performed deformation tests on a variety of Si_3N_4 -based ceramics with submicrometer-sized microstructures in the SPS apparatus and, for the sake of comparison, in a conventional hot-pressing (HP) furnace, and we observed a radical improvement in the deformation rate when the SPS apparatus was used. Below, we will present two representative examples.

Two materials, one α - and one β -sialon, isostructural with α - Si_3N_4 and β - Si_3N_4 , respectively, with overall compositions of $\text{Y}_{0.175}\text{Yb}_{0.175}\text{Si}_{9.75}\text{Al}_{2.25}\text{O}_{1.64}\text{N}_{14.54}$ and $\text{Y}_{0.01}\text{Si}_{1.91}\text{Al}_{0.215}\text{O}_{0.166}\text{N}_{2.66}$, were consolidated to full density by the SPS process at 1500 °C and 1550 °C, respectively. Respective holding times of 2 and 4 min were used under a uniaxial pressure of 50 MPa. The compacts obtained consisted of fine, equi-axed grains with average sizes of 210 and 350 nm, respectively, and